

Design and Analysis of Linear Taper Directional Couplers

Yasser Gharbi, and Adnan Affandi

Electrical and Computer Engineering Department King Abdul Aziz University
ygharbi999@yahoo.com

Abstract: Coupled Linear transmission lines in inhomogeneous media are analyzed. The solution is used to design microwave directional couplers. The designed couplers have much improved coupling characteristics compared with couplers using uniform lines. Also in this work, the neural network is employed as a tool in design of the LDCTL. [Adnan Affandi, Yasser Gharbi. **Design and Analysis of Linear Taper Directional Coupler.** *Life Sci J* 2015;12(4):139-152]. (ISSN:1097-8135). <http://www.lifesciencesite.com>. 18

Keywords: Linear Taper; Directional Coupler

1. Introduction

Non-uniform transmission lines have considerable applications in microwave circuits such as resonators, transformers, matching sections and filters [1-4]. Normally the TEM mode of propagation in the non-uniform transmission line is described by its non-constant characteristic impedance which varies along the direction of propagation of electromagnetic waves. This property made the non-uniform transmission lines responses superior to those of uniform ones.

Usually the exact network functions of general non-uniform transmissions are not known except for few cases such as binomial transmission lines (including linear and parabolic tapers) exponential, triangular and radial transmission lines [5-10]. Uniform & Non-uniform transmission lines could be isolated or coupled.

Coupled uniform transmission lines are used in the realization of various types of microwave circuits i.e. filters, frequency discriminator, directional couplers, phase shifters and impedance transformers. Coupled non-uniform transmission line, by its nature of non-uniformity, offers additional design parameters to achieve the desired device performance, inherent impedance transformation capabilities and the possibility of the realization of a wide band components. Therefore non-uniform transmission line directional couplers can provide both broadband capability and transmission responses superior to the uniform ones [11,12].

These coupler may serve as building blocks for phase shifters, mixers, multiplexers, balances and duplexers which are essential and required in multi-octave bandwidth antenna and broadband microwave systems [13-16].

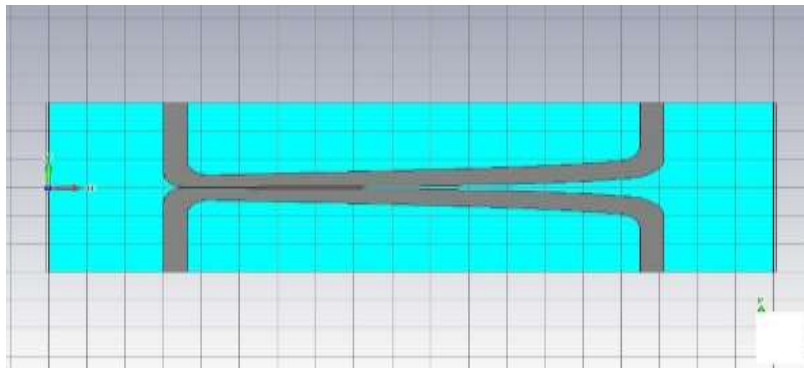


Figure 1. Linear taper directional coupler transmission line (LDCTL)

2. Analysis of Lossy CLTL In Inhomogeneous Media

Kobaya K. Shi, Nemoto Y. and R. Sato derived expressions for the first order differential equations for the voltage and current which describe the lossless binomial transmission line [17,18]. One of the purposes of this paper is to derive

expressions for differential equations for the voltage and the current which govern the lossy coupled binomial transmission line (CBTL) in inhomogeneous media see fig.1, and then utilize their solutions to derive the ABCD matrix for CBTL [19-22]. The electrical properties of the lossy CBTL vary as follows:

$$L0_{e,o} = L1_{e,o} (k)^{2ne,o}, R0_{e,o} = R1_{e,o} (k)^{2ne,o}, C0_{e,o} = C1_{e,o} (k)^{2ne,o} \text{ and } G0_{e,o} = G1_{e,o} (k)^{2ne,o}$$

where $L0_{e,o}$, $R0_{e,o}$, $C0_{e,o}$ and $G0_{e,o}$ are the even and odd mode inductance, resistance, capacitance and conductance respectively at $x = 0$, and the subscript e and o refer to the even and odd modes respectively.

The first order differential equations for the voltage and current which describe the Lossy CBTL may be expressed as:

$$-\frac{dV_{e,o}(x)}{dx} = Z1_{e,o} \gamma_{e,o} (k+x)^{2ne,o} * I_{e,o}(x) \quad (1)$$

$$-\frac{dI_{e,o}(x)}{dx} = \frac{\gamma_{e,o}}{Z1_{e,o}} (k+x)^{-2ne,o} V_{e,o}(x) \quad (2)$$

where $\gamma_{e,o}$ is the even and odd propagation constant which may be written as:

$$\gamma_{e,o} = \sqrt{(R1_{e,o} + j\omega L1_{e,o})(G1_{e,o} + j\omega C1_{e,o})} \quad (3)$$

While the even and odd mode characteristic impedance may be expressed as:

$$Z1_{e,o} = Z0_{e,o} (k)^{-2ne,o} \quad (4)$$

By differentiating equations (1) and (2) with respect to x and then letting $y = (k_{e,o} + x)$ and then multiplying by y^2 , the following second order differential equations for the voltage and current may be obtained:

$$y^2 \frac{d^2 V_{e,o}(y)}{dy^2} - 2n_{e,o} * y \frac{dV_{e,o}(y)}{dy} + (j\gamma_{e,o} * y)^2 * V_{e,o}(y) = 0 \quad (5)$$

$$y^2 \frac{d^2 I_{e,o}(y)}{dy^2} - 2n_{e,o} * y \frac{dI_{e,o}(y)}{dy} + (j\gamma_{e,o} * y)^2 * I_{e,o}(y) = 0 \quad (6)$$

These differential equations are called Bessel's differential equations and their solution will be in the following form:

$$V_{e,o}(y) = K1_{e,o} * y^{(2ne,o+1)/2} * J_{(2ne,o+1)/2}(-j\gamma_{e,o}y) - (-1)^n * K2_{e,o} * y^{(2ne,o+1)/2} * J_{(2ne,o+1)/2}(-j\gamma_{e,o}y) \quad (7)$$

$$I_{e,o}(y) = K3_{e,o} * y^{-(2ne,o-1)/2} * J_{(2ne,o-1)/2}(-j\gamma_{e,o}y) + (-1)^n * K4_{e,o} * y^{-(2ne,o-1)/2} * J_{-(2ne,o-1)/2}(-j\gamma_{e,o}y) \quad (8)$$

where:-

$$K1_{e,o} = (-1)^n * \left(\sqrt{\frac{-j\pi\gamma_{e,o}}{2}} \right)^2 * K^{-(2ne,o-1)/2} * J_{-(2ne,o-1)/2}(-j\gamma_{e,o}K) * V0_{e,o} + j Z1_{e,o} * K^{(2ne,o-1)/2} * J_{-(2ne,o+1)/2}(-j\gamma_{e,o}K) * I0_{e,o} \quad (9)$$

$$K2_{e,o} = \left(\sqrt{\frac{-j\pi\gamma_{e,o}}{2}} \right)^2 * \{-K^{(2ne,o-1)/2} * J_{(2ne,o-1)/2}(-j\gamma_{e,o}K)\}$$

$$V4_{e,o} + j Z1_{e,o} * K^{(2ne,o+1)} * J_{(2ne,o+1)/2}(-j\gamma_{e,o}K) * I0_{e,o} \quad (10)$$

$$K3_{e,o} = -j \frac{K1}{Z1_{e,o}} \text{ \& } K4_{e,o} = -j \frac{K2}{Z1_{e,o}} \quad (11)$$

By substituting $x = \frac{1}{k} & y = K + \frac{1}{k}$ into equations (7) and (8). Therefore equations (7) and (8) becomes as:

$$V1_{e,o} = T_{e,o} * M_{e,o} * \left\{ J_{-(2ne,o-1)/2}(-j\gamma_{e,o}K) * J_{(2ne,o+1)/2}(-\gamma_{e,o}(K + \frac{1}{k})) \right\}$$

$$\begin{aligned}
 & + J_{(2ne, o-1)/2} (-j \gamma_{e,o} K) * \\
 & J_{-(2ne, o+1)/2} (-j \gamma_{e,o} (K+1)) * V_{0e,o} \\
 & + j Z_0 \{ J_{-(2ne, o+1)/2} (-j \gamma_{e,o} K) * \\
 & J_{(2ne, o+1)/2} (-j \gamma_{e,o} (K+1)) \\
 & - J_{(2ne, o+1)/2} (-j \gamma_{e,o} K) * J_{-(2ne, o+1)/2} \\
 & (-j \gamma_{e,o} (K+1)) * I_{0e,o} \} \quad (12)
 \end{aligned}$$

$$\begin{aligned}
 I_{e,o} &= \frac{T_{e,o}}{M_{e,o}} * \left\{ -j \frac{1}{Z_{0e,o}} \{ \right. \\
 & J_{-(2ne, o-1)/2} (-j \gamma_{e,o} K) * J_{(2ne, o-1)/2} (-j \\
 & (K+1)) - J_{(2ne, o-1)/2} (-j \gamma_{e,o} K) * \\
 & J_{-(2ne, o+1)/2} (-j \gamma_{e,o} (K+1)) * V_{0e,o} \\
 & + \left. \left\{ J_{-(2ne, o+1)/2} (-j \gamma_{e,o} K) * \right. \right. \\
 & J_{(2ne, o-1)/2} (-j \gamma_{e,o} (K+1)) \\
 & + \left. \left. J_{(2ne, o+1)/2} (-j \gamma_{e,o} K) * J_{-(2ne, o-1)/2} \right. \right. \\
 & \left. \left. (-j \gamma_{e,o} (K+1)) * I_{0e,o} \right\} \quad (13)
 \end{aligned}$$

where is:-

$$\begin{aligned}
 T_{e,o} &= (-I)^n \sqrt{\frac{-j\pi\gamma_{e,o}K}{2}} * \sqrt{\frac{-j\pi\gamma_{e,o}(K+1)}{2}} \\
 \text{and } M_{e,o} &= \left(\frac{K+1}{K}\right)^n \quad (14)
 \end{aligned}$$

The even and odd mode voltages and currents can be easily written in the matrix form as follows:

$$\begin{bmatrix} V_{1e,o} \\ I_{1e,o} \end{bmatrix} = \begin{bmatrix} F \\ \end{bmatrix} \begin{bmatrix} V_{0e,o} \\ I_{0e,o} \end{bmatrix} \quad (15)$$

where

$$\begin{bmatrix} F \\ \end{bmatrix} = \begin{bmatrix} F_1 & F_3 \\ F_2 & F_4 \end{bmatrix}$$

and

$$\begin{aligned}
 F_1 &= T_{e,o} * M_{e,o} \left\{ J_{-(2ne, o-1)/2} (-j \gamma_{e,o} K) \right. \\
 & * J_{(2ne, o+1)/2} (-\gamma_{e,o} (K+1)) \\
 & + J_{(2ne, o-1)/2} (-j \gamma_{e,o} K) * \\
 & J_{-(2ne, o+1)/2} (-j \gamma_{e,o} (K+1)) \left. \right\} \\
 F_2 &= \frac{T_{e,o}}{M_{e,o}} * \left\{ -j \frac{1}{Z_{0e,o}} \left\{ J_{-(2ne, o-1)/2} \right. \right. \\
 & (-j \gamma_{e,o} K) * J_{(2ne, o-1)/2} (-j \gamma_{e,o} \\
 & (K+1)) - J_{(2ne, o-1)/2} (-j \gamma_{e,o} K) * \\
 & J_{-(2ne, o+1)/2} (-j \gamma_{e,o} (K+1)) \left. \right\} \\
 F_3 &= j Z_0 \left\{ J_{-(2ne, o+1)/2} (-j \gamma_{e,o} K) * \right. \\
 & J_{(2ne, o+1)/2} (-j \gamma_{e,o} (K+1)) \\
 & - J_{(2ne, o+1)/2} (-j \gamma_{e,o} K) * J_{-(2ne, o+1)/2} \\
 & (-j \gamma_{e,o} (K+1)) \left. \right\} \\
 F_4 &= \left\{ J_{-(2ne, o+1)/2} (-j \gamma_{e,o} K) * \right. \\
 & J_{(2ne, o-1)/2} (-j \gamma_{e,o} (K+1)) \\
 & + J_{(2ne, o+1)/2} (-j \gamma_{e,o} K) * \\
 & J_{-(2ne, o-1)/2} (-j \gamma_{e,o} (K+1)) \left. \right\}
 \end{aligned}$$

Equation (15) may also be expressed as:-

$$\begin{bmatrix} V_{0e,o} \\ I_{0e,o} \end{bmatrix} = \begin{bmatrix} A_{e,o} & B_{e,o} \\ C_{e,o} & D_{e,o} \end{bmatrix} \begin{bmatrix} V_{1e,o} \\ I_{1e,o} \end{bmatrix} \quad (16)$$

where

$$A_{e,o} = \frac{T_{e,o}}{M_{e,o}} \left\{ J_{-(2ne,o+1)/2} (-j \gamma_{e,o} K) \right. \\ \left. * J_{(2ne,o-1)/2} \right.$$

$$K) * (-j \gamma_{e,o} (K + 1)) + J_{(2ne,o+1)/2} (-j \gamma_{e,o} K) \\ \left. * J_{-(2ne,o-1)/2} (-j \gamma_{e,o} (K + 1)) \right\}$$

$$B_{e,o} = j Z_{0e,o} * T_{e,o} * M_{e,o} * \left\{ J_{-(2ne,o+1)/2} (-j \gamma_{e,o} K) \right. \\ \left. * J_{(2ne,o+1)/2} \right.$$

$$(-j \gamma_{e,o} (K + 1)) - J_{(2ne,o+1)/2} (-j \gamma_{e,o} K) * \\ \left. J_{-(2ne,o+1)/2} \right.$$

$$* (-j \gamma_{e,o} (K + 1)) \left\{ \frac{1}{Z_{0e,o}} * \frac{T_{e,o}}{M_{e,o}} \right. \\ \left. * J_{-(2ne,o-1)/2} \right. \\ \left. (-j \gamma_{e,o} K) * J_{(2ne,o-1)/2} \right.$$

$$* (-j \gamma_{e,o} (K + 1)) - J_{(2ne,o-1)/2} (-j \gamma_{e,o} K) * \\ \left. J_{-(2ne,o+1)/2} \right.$$

$$* (-j \gamma_{e,o} (K + 1)) \left\{ T_{e,o} * M_{e,o} \right. \\ \left. * J_{-(2ne,o-1)/2} (-j \gamma_{e,o} K) * J_{(2ne,o+1)/2} \right.$$

$$* (-j \gamma_{e,o} (K + 1)) + J_{(2ne,o-1)/2} (-j \gamma_{e,o} K) * \\ \left. J_{-(2ne,o+1)/2} \right.$$

$$* (-j \gamma_{e,o} (K + 1)) \left. \right\} \quad (17)$$

To find the A, B, C & D parameters for a parabolictaper two port transmission line of the second degrees we put n = i.e. the following relevant parameters must be defined:

$$\gamma_{e,o} = \alpha + j\beta_{e,o} \quad (18)$$

$$h = \frac{K}{\ell} \quad (19)$$

$$m = \frac{(1+h)}{h} \quad (20)$$

where α is the attenuation constant $\beta_{e,o}$ is the phase constant, h is the taper rate and ℓ is the electrical length of the coupler. For lossless case i.e. $\alpha = 0$ and for n = 1, the ABCD linear taper parameters can be expressed as:

$$A_{e,o} = \frac{1}{m} \left(\cos \beta_{e,o} \ell + \frac{\sin \beta_{e,o} \ell}{\beta_{e,o} \ell} \right)$$

$$B_{e,o} = j m * Z_{0e,o} \left[\sin \beta_{e,o} \ell - \frac{1}{h(h+1)} * \right. \\ \left. \frac{1}{\beta_{e,o} \ell} * \left(\frac{\sin \beta_{e,o} \ell}{\beta_{e,o} \ell} - \cos \beta_{e,o} \ell \right) \right]$$

$$C_{e,o} = j \frac{1}{m Z_{0e,o}} \sin \beta_{e,o} \ell$$

$$D_{e,o} = m \left(\cos \beta_{e,o} \ell - \frac{1}{h(h+1)} * \left(\frac{\sin \beta_{e,o} \ell}{\beta_{e,o} \ell} \right) \right)$$

3. The Scattering Matrix Parameters

First of all the even and odd mode $A_{e,o}$, $B_{e,o}$, $C_{e,o}$, $D_{e,o}$ matrices for the lossy non-uniform coupled lines must be derived. These are then used to calculate the reflection and transmission coefficients, in terms of which the scattering parameter matrix can then be written. The even and odd mode reflection and transmission coefficients for the non-uniform directional couplers are obtained as:-

$$\rho_{e,o} = \frac{Z_{L_{e,o}} A_{e,o} + B_{e,o} - Z_{L_{e,o}} Z_{S_{e,o}} C_{e,o} - Z_{S_{e,o}} D_{e,o}}{Z_{L_{e,o}} A_{e,o} + B_{e,o} + Z_{L_{e,o}} Z_{S_{e,o}} C_{e,o} + Z_{S_{e,o}} D_{e,o}} \quad (22)$$

$$\tau_{e,o} = \frac{2}{Z_{L_{e,o}} A_{e,o} + B_{e,o} + Z_{L_{e,o}} Z_{S_{e,o}} C_{e,o} + Z_{S_{e,o}} D_{e,o}} \quad (23)$$

The scattering parameters for CBTL when the input signal either introduced at port (1) or port (2) (fig. 1) may be expressed as:

$$S_{22}=S_{11} = \rho_e \frac{1}{2} + \frac{1}{2} \rho_o \quad (24)$$

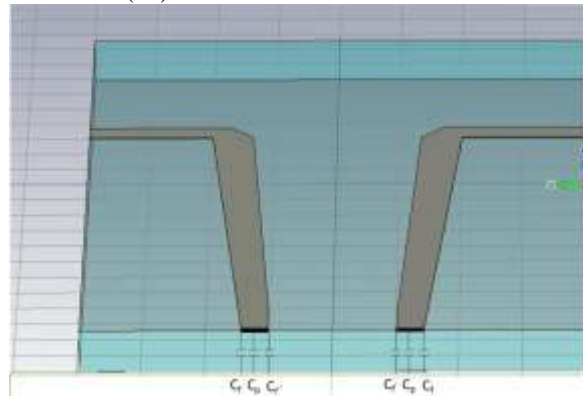


Fig. 2a show the capacitances representation of the even mode field distribution for zero conductor thickness

Goergand R. Bahi I. J. [11] derive expressions for the even and odd mode capacitances respectively as: (fig. 2).

$$C_e = C_p + C_f + C'f \quad (28)$$

$$C_o = C_p + C_f + C_{ga} + C_{gd} \quad (29)$$

Where

$$C_p = \frac{\epsilon_o \epsilon_r W}{h} \quad (30)$$

Where $\epsilon_o = 2.25 \times 10^{-4} \text{ pF/cm}$ ϵ_r is the dielectric constant of the material under investigations, while C_f , $C'f$, C_{ga} and C_{gd} were calculated and defined in reference [12].

$$S_{12}=S_{21} = \frac{1}{2} \tau_e + \frac{1}{2} \tau_o \quad (25)$$

$$S_{42}=S_{31} = \frac{1}{2} \rho_e - \frac{1}{2} \rho_o \quad (26)$$

$$S_{32}=S_{41} = \frac{1}{2} \tau_e - \frac{1}{2} \tau_o \quad (27)$$

The same procedure can be applied in calculating the scattering parameters when the input signals are applied at either port (3) or (4).

4. Determination Of Non-Uniform Microstrip Coupled Line Parameters

Usually in designing procedure of the non-uniform microstrip coupled lines, the parameters which characterize these structure must be determined. These parameters include the even and odd mode capacitances, impedances, effective dielectric constants and phase velocities of propagation [23,24].

5. Calculation Of The Even And Odd Mode Capacitances

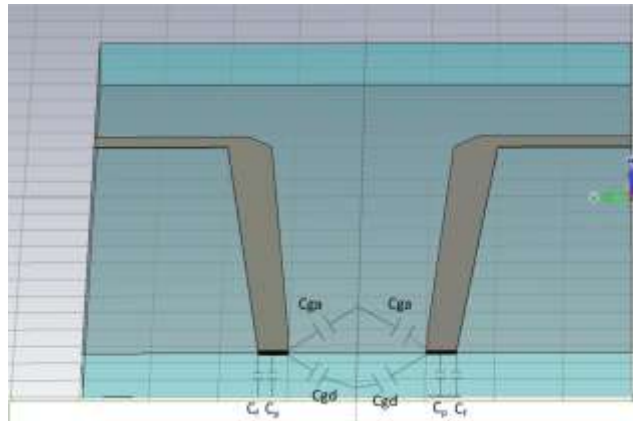


Fig. 2b show the capacitances representation of the odd mode field distribution for zero conductor thickness

Fig 2 illustrates the capacitances representing of the even and odd mode electrical field distribution. Wand h are the width of the single conductor and the thickness of the substrate respectively. Saeed Al

Bodare improved equation (28)[2]by adding the fringing capacitance $C'f$ to the odd mode equation.

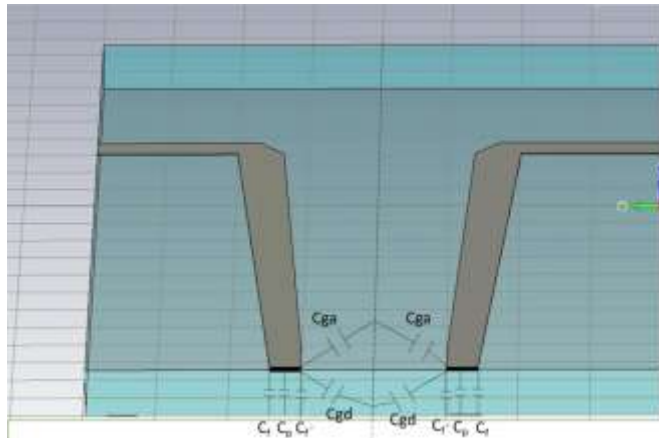


Fig. 3.The odd mode capacitance representation of the electric field distribution for zero conductor thickness.

Fig. 3 show the capacitances representing the improved odd mode electrical field distribution with

$C'f$ included.

$$C_o = C_p + C_f + C'f + C_{ga} + C_{gd} \quad (31)$$

Where $C'f$ is the fringing capacitance which was derived and defined in reference [13], [15]. Further improvement to equations (1) and (2) have been made by Dalby A.B. [14] by including the extra fringing capacitance which was caused by non-zero conductor thickness (fig. 4.).

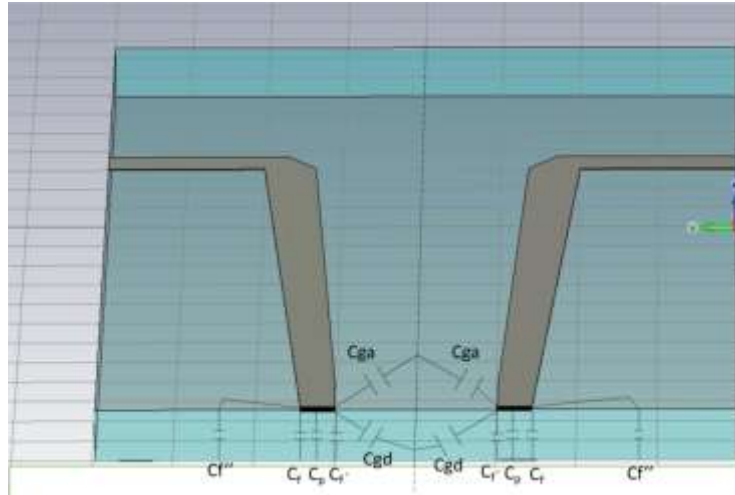


Fig. 4.Improved capacitor representation of the odd mode electric field distribution.

Therefore equations (27) and (30) can be written [16] as:

$$C_o = C_p + C_f + C'_f + C''_f + C_{ga} + C_{gd} \quad (33)$$

$$C_e = C_p + C_f + C'_f + C''_f \quad (32)$$

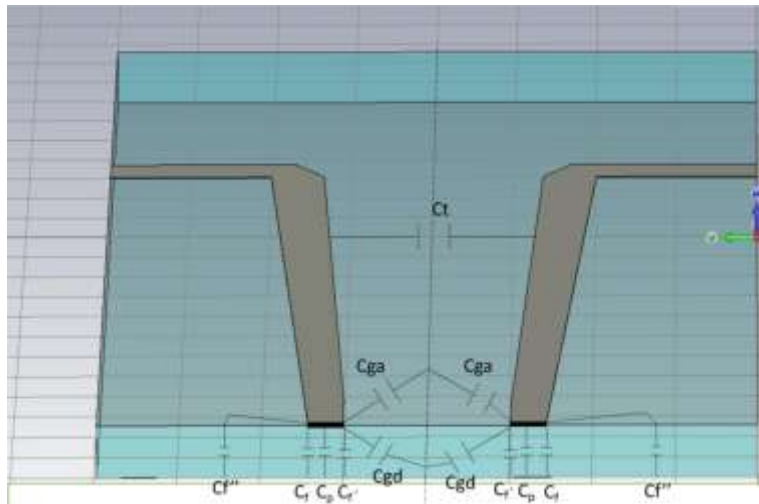


Fig. 5. The extra improvement in the odd mode electric field distribution.

Fig.4 shows the accurate decomposition of the odd mode capacitances.

where C''_f was defined and derived in reference [17]. Also further improvement has been made to equation (32) by including the extra odd mode air capacitance which was also attributed to the non-zero conductor thickness

[6]. Therefore equation (32) becomes as:

$$C_o = C_p + C_f + C'_f + C''_f + C_t + C_{ga} + C_{gd} \quad (34)$$

where C_t is the increase in odd mode air capacitance which can be written for the uniform coupled line as:

$$C_t = \frac{\epsilon_o TL}{S} \quad (35)$$

where T is the finite thickness of the conductor, L is the length of the conductor and S is the separation between the coupled lines. Equation (35) can be modified for non-uniform coupled lines as:

$$C_{t \text{ nonuniform}} = \frac{\varepsilon_o TL}{\sum_{n=0}^{n=100} [S_o \pm n(2\Delta S_n)]} \quad (36)$$

Where the positive sign of $+2\Delta S_n$ indicates the incremental increase in the spacing between the coupled line obtained at the tight coupling end while the negative sign of $-2\Delta S_n$ indicates the incremental decrease in the spacing as one move from the loose coupling side to the tight coupling end. [26,27,28] Fig.5 shows how the computation of the spacing between the non-uniform coupled line has been done.

6. The even And The Odd Mode Characteristic Impedances

The characteristic impedances for the two modes can be obtained from the capacitance value, using the following relations [14]

$$Z_{oe} = \frac{1}{V\sqrt{C_e C^a_e}} \quad (37)$$

$$\text{And } Z_{oo} = \frac{1}{V\sqrt{C_o C^a_o}} \quad (38)$$

Where V is the velocity of the waves in air, while C^a_e and C^a_o denotes the even and odd capacitances with air as dielectric.

7. The Even And Odd Mode Effective Dielectric Constants

The effective dielectric constants of the even and odd mode can be expressed as: [18]

$$\varepsilon^e_{re} = \frac{C_e}{C^a_e} \quad (39)$$

$$\varepsilon^o_{re} = \frac{C_o}{C^a_o} \quad (40)$$

The hybrid effective dielectric constant may be written as: [19]

$$\varepsilon_{eff} = \left(\frac{\sqrt{\varepsilon^e_{re}} + \sqrt{\varepsilon^o_{re}}}{2} \right)^2 + 0.082 \quad (41)$$

Once the material substrate is defined and the even and odd mode capacitances are computed, the cross sectional area dimension of the non-uniform couplers can be easily calculated at the central frequency as:

$$L = \frac{\lambda_o}{4\sqrt{\varepsilon_{eff}}} \quad (42)$$

Where λ_o is the free space wave length.

8. General design procedure

In microstrip, the nonuniform coupled lines, are faced with the problem of different phase velocities for the even and odd modes of propagation. In microstrip coupled lines, uniform or nonuniform, the inequality in the phase velocities of the even and odd mode usually caused low directivity and return loss. Therefore a perfect coupler with effect matching and infinite directivity is not achievable in practice. Thus the amount of parameter tolerance need to be specified in the initial stage of directional coupler design.

The initial specifications for the required directional coupler are:

- 1) Coupling factor, say, $C = -10 \pm 0.45$ dB
- 2) Single microstrip feed line characteristic Impedances $Z_o = 50 \Omega$
- 3) Substrate permittivity ε_r , and thickness of the substrate h,
- 4) $\frac{T}{h}$ Ratio of the conductor thickness to substrate thickness.
- 5) Dielectric constant Teflon: $\varepsilon_r = 2.3$ or Alumina: $\varepsilon_r = 9.7$
- 6) The operating frequency $f_o = 12$ GHz
- 7) Lowest acceptable isolation $I = -30$ dB
- 8) Mismatch acceptable = -30 dB
- 9) Transmission $\tau = 0$ dB

The approximate condition for minimum input mismatch and maximum isolation is as follows [18]:

$$Z_o^2 = Z_{oe}(x) * Z_{oo}(x) \quad (43)$$

as given in [18].

9. Design procedure for Linear taper directional coupler (CLTL)

In the design of a linear directional coupler we can assume that the equation (43) is satisfied if the even and odd modes rate of taper are chosen to be

$$h_e = h_o = h$$

where

$$h = \frac{Z_o}{Z_L - Z_o} \tag{44}$$

where Z_o & Z_L are respectively the input and output impedance and the even mode impedance is

$$Z_{eo}(x) = Z_{eo}(0) \left(1 + \frac{X_L}{h}\right) \tag{45}$$

while the odd mode impedance is:

$$Z_{oo}(x) = Z_{oo}(0) \left(1 + \frac{X_L}{h}\right) \tag{46}$$

Thus the condition for best performance of this coupler becomes

$$Z_o^2 = Z_{oe}(x) * Z_{oo}(x) \tag{47}$$

10. The Performance of The Coupled Linear Directional Couplers

The CLTL directional couplers were fabricated on three identical substrates of dielectric constant $\epsilon_r = 10$ and thickness $h = 0.635$ mm with coupling specification of 10.25 ± 0.45 dB. These couplers were designed to operate at 3.5 GHz with acceptable bandwidth of 10%. In figures 6&7 are shown the typical frequency responses of the computed and measured scattering responses of the computed and measured scattering matrix-parameters of S_{11} , S_{21} , S_{31} , S_{41} and S_{14} , S_{24} , S_{34} , S_{44} , when the input signals were introduced at ports (1) and (4) respectively.

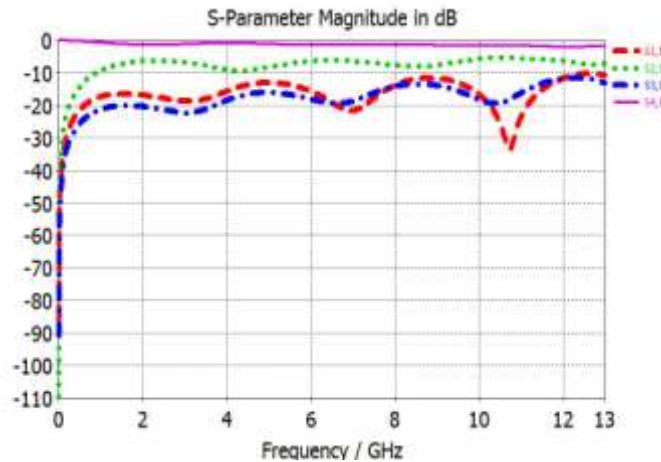


Fig. 6. The scattering parameters S_{11} , S_{21} , S_{31} , S_{41} of a CETL directional coupler in an inhomogeneous medium.

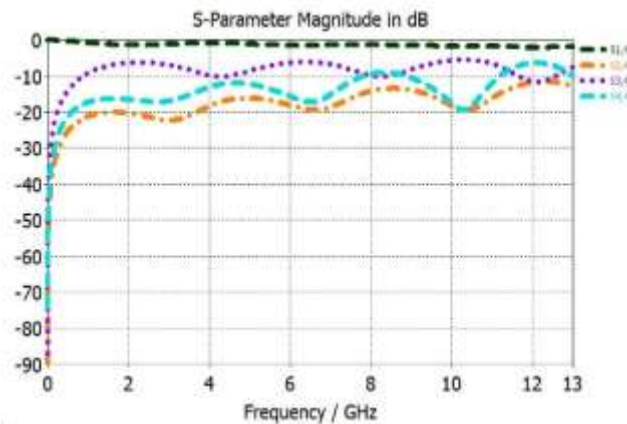


Fig. 7. The scattering parameters S_{14} , S_{24} , S_{34} , S_{44} of a CLTL directional coupler in an inhomogeneous medium.

Because of the symmetry, the remaining scattering parameters of S_{12} , S_{22} , S_{32} , S_{42} and S_{13} , S_{23} , S_{33} , S_{34} when the input signal were applied at

ports (2) and (3) respectively are not required. Figs. 6&7 show that very good agreement between the optimized and measured values were obtained.

A high frequencies the isolations of the proposed non-uniformed directional couplers deteriorate due to the difference in the even and odd mode velocities.

11. Development of Neural Network

Neural network as the name sounds is interconnection of nerve cells. The artificial neural network technology is built up with an inspiration of functioning of human nervous system. Many of human intelligent behavior which is the direct functioning of human nervous system are implemented artificially in artificial neural network. It is inspired by the way biological nervous systems works. It is composed of a large number of highly interconnected processing elements called neurons working in union to solve specific problems. Like human, artificial neural network also learn by example. It is configured for specific application, such as pattern recognition or data classification through learning process. Learning involves adjustments to the synaptic connection known as weights that exist between the neuron. In artificial neural network, the information processing elements are known as nodes. The first layer of nodes is known as input layer. Whereas the last layer is known as output layer. The layers in between which may or may not exist is known as hidden layer(s). The information is transmitted by means of connecting links. The links possess an associated weight, which is multiplied with the incoming signal for any typical neural network. The output is obtained by applying activations to the net. Artificial neural network is used to train computers to do various operations which need human intelligence. There are various categories of artificial neural networks used for training computers for specific category of work. Among the single layered networks there are Perceptron Model, Associative Network, Adaline Network Madaline Network, Hoffield Network whereas in multilayered network we have Back Propagation model, radial basis network, self organizing map, learning vector quantization etc.[20].

12.1 Estimation of Linear

Radial Basis Function Neural Networks (RBFNN) algorithm (2) recursive is used to estimate exponential directional coupler transmission line. The construction of RBF network, in its most basic form, involves three layers with entirely different roles. The input layer is made up of source nodes (sensory units) that connect the network to its environment. The second layer, the only hidden layer in the network applies a nonlinear transformation from the input space to the hidden space. In most applications the hidden space is of high dimensionality. The output layer is linear, supplying the response of the network to the activation pattern applied to the input layer. A

RBF net architecture is given in figure 8. Radial Basis function networks are substantially faster than the methods used to train multi-layer perceptron networks. This follows from the interpretations which can be given to the internal representation formed by the hidden units, and leads to a two stage training procedure. In the first stage, the parameters governing the basis functions (corresponding to hidden units) are determined using relatively fast, unsupervised methods, in which it uses only input data and not the target data. The second stage of training then involves the determination of the final-layer weights, which requires the solution of a linear problem, and which is therefore also fast. The trained neural network provides a special approximation where the exact results of the numerical analysis, which are hidden in the training patterns, are used for neural computation and give us directly all the required designing parameter of an antenna for a desired frequency. That way, a computationally modest neural network model can replace a numerical analysis for parameters differing from training patterns.

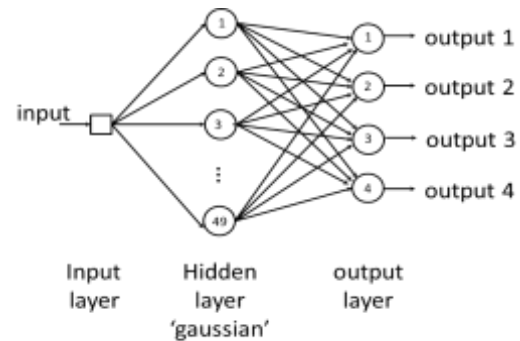


Fig. 8. RBFNN algorithm (2) recursive

12.2 RBFNN algorithm (2) recursive Architecture

In fig 8 first layer is called as input layer where external information is received and is consisted of 1 input frequency f in GHz. The middle layer consist of 49 neurals with Gaussian activation function. The last layer is called as output layer where the network produces the model estimation and is consisted of 4 outputs and S_{11} , S_{21} , S_{31} and S_{41} . Fig. 8 shows the result of estimation graph. The accuracy of the RBFNN technique was evaluated by comparing the predicted solutions from our neural network to those from a published paper [1]. Fig. 8 show an excellent agreement between the results provided by Koboyashi K., Nemoto Y. [1] and the RBFNN.

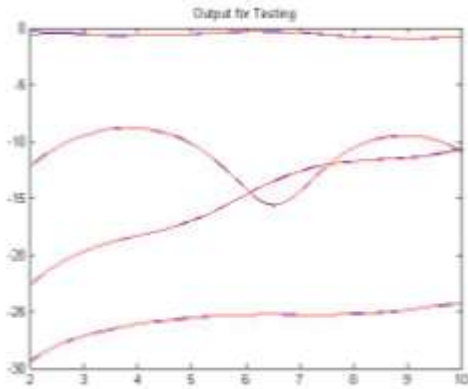


Fig. 9. The scattering parameters of [1] and Estimation.

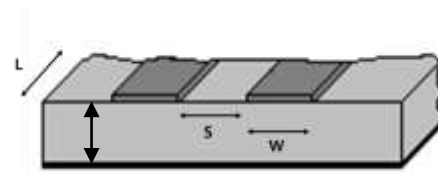


Fig. 10. physical dimensions of EDCTL

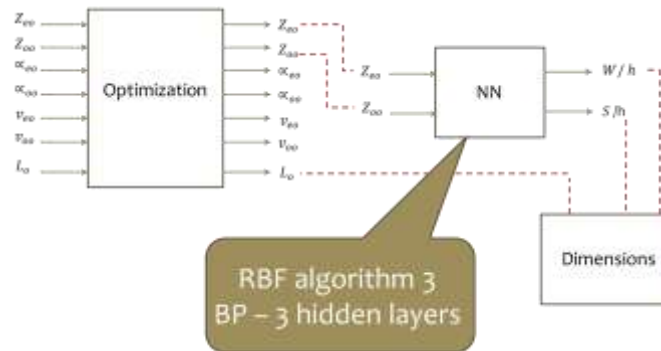


Fig. 11. Finding physical dimension using Optimization and Neural Network

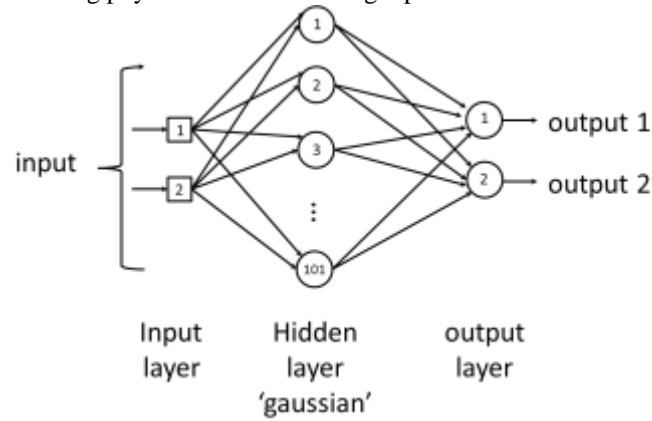


Fig. 12. RBFNN algorithm (3)

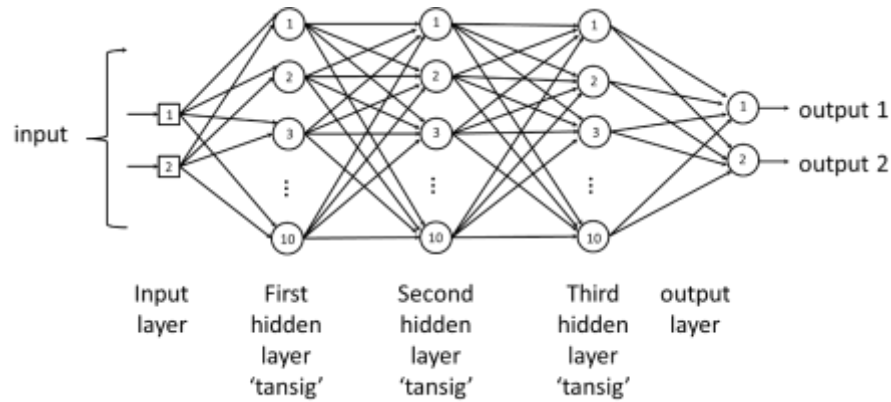


Fig. 13. BPNN

12.3 Finding physical dimensions using Optimization and Neural Network

In this paper, two types of neural network have been used to find the physical dimensions of the exponential directional coupler (w/h and s/h). First type is Radial Basis Function Neural Networks (RBFNN) algorithm (3). Architecture structure is shown in fig, 12. Second type is Back Propagation neural network (BPNN). For designing this type of neural network we use nn tool in matlab software. Architecture structure is shown in fig, 13. RBFNN algorithm (3) in fig. 10 is consists of 3 layers. First layer is called as input layer where Z_{eo} and Z_{oo} are received. The middle layer consist of 101 neurals with Gaussian activation function. The output layer is

consisted of 2 neurals w/h and s/h. BPNN in fig. 12 is consist of 3 layers. The input layer has 2 neurals Z_{eo} and Z_{oo} . The middle layer is made of three hidden layers and 10 neurals in each hidden layer with tensing activation function. The output layer is consisted of 2 neurals w/h and s/h. The both neural networks are trained with data set of various values of Z_{eo} , Z_{oo} , w/h and s/h. Once you have trained the network, choose Z_{eo} , Z_{oo} to simulate, for which design parameters are to find, It can calculatr the design constraints close to optimum value of w/h and s/h. Simulated results are shown below (see fig. 14):-

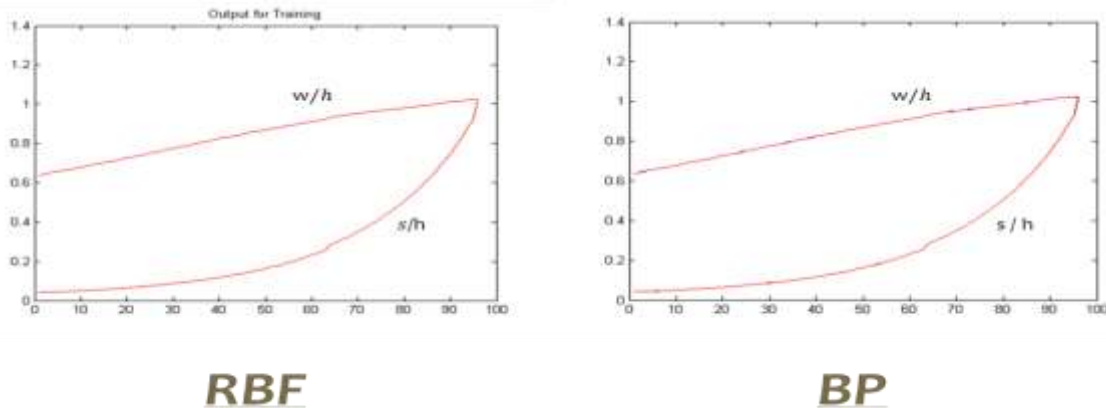


Fig. 14 The output of training of RBFNN and BPNN

For RBFNN
 $w/h = 1.5125$
 $s/h = 0.1548$
 $L = 2.5$ mm
 For BPNN
 $w/h = 1.5251$
 $s/h = 0.1418$
 $L = 2.5$ mm

The dimensions of LDCTL calculated by RBFNN and BPNN are very close to each other.

Conclusion

The solution derived for the characterization of CLTL in inhomogeneous media gives good design parameters for microwave couplers. Microstrip couplers using LDCTL have a much flatter frequency

response than those using uniform lines. The use of neural network for transmission line analysis opens the way to a significant improvement in design efficiency. Moreover, nothing prevents this technique to be applied to more complex structures, like non-symmetric transmission line or even multi-mode waveguides. The analysis of nonuniform waveguides is a problem for which there are currently no simple and efficient solutions. The proposed technique has great potential to provide answers in this area. We have presented a technique to compute the scattering parameters of a nonuniform symmetrical transmission line by using an artificial neural network. Also in this work, the neural network is employed as a tool in design of the LDCTL. In this design procedure, synthesis is defined as the forward side. Therefore, one can obtain the geometric dimensions with high accuracy, i.e. w/h and s/h in our geometry, at the output of the synthesis network by inputting Z_{eo} and Z_{oo} .

References

1. Koboyashi K., Nemoto Y., and Sato R. "Equivalent circuits of binomial form non uniform transmission lines and their application," Trans. IECE, Japan, volume. 63-a, number (11):, pages. 807- 814, November 1980.
2. Rehman, A. and Saba, T. (2011). Document skew estimation and correction: analysis of techniques, common problems and possible solutions Applied Artificial Intelligence, vol. 25(9), pp. 769-787. doi. 10.1080/08839514.2011.607009
3. Rehman,A., Saba, T. (2011)Performance analysis of character segmentation approach for cursive script recognition on benchmark database, Digital Signal Processing, vol. 21(3),pp. 486-490, doi.10.1016/j.dsp.2011.01.016.
4. Saba,T., and Altameem, A. (2013) Analysis of vision based systems to detect real time goal events in soccer videos, Applied Artificial Intelligence, vol.27(7), pp. 656-667.
5. Affandi A. M., Mahdi S., Almoabadi M., " Analysis of some non-uniform transmission lines with selected applications " ICECS`94, pages. 153-162, December 19-22, 1994, Cairo, EGYPT.
6. Ahmad, AM., Sulong, G., Rehman, A., Alkawaz,MH., Saba, T. (2014) Data Hiding Based on Improved Exploiting Modification Direction Method and Huffman Coding, Journal of Intelligent Systems, vol. 23 (4), pp. 451-459, doi. 10.1515/jisys-2014-0007.
7. Harouni, M., Rahim, MSM., Al-Rodhaan,M., Saba, T., Rehman, A., Al-Dhelaan, A. (2014) Online Persian/Arabic script classification without contextual information, The Imaging Science Journal, vol. 62(8), pp. 437-448, doi. 10.1179/1743131X14Y.0000000083.
8. Meethongjan,K. Dzulkifli,M. Rehman,A. Altameem,A. Saba, T. (2013) An intelligent fused approach for face recognition, Journal of Intelligent Systems vol.22(2), pp. 197-212.
9. Haron, H. Rehman, A., Wulandhari, L.A., Saba, T. (2011) Improved vertex chain code based mapping algorithm for curve length estimation, Journal of Computer Science vol. 7(5), pp. 736-743.
10. Saba, T. Rehman, A. Altameem, A. Uddin, M. (2014) Annotated comparisons of proposed preprocessing techniques for script recognition, Neural Computing and Applications, vol. 25(6), pp. 1337-1347 , doi. 10.1007/s00521-014-1618-9
11. Meaney P., "A Novel Branch - Line Coupler Design For Millimeter - Wave Applications " IEEE MTT - S Digest, Number 0 - 4 pages 585 - 588, 1990.
12. Rehman, A., and Saba, T. (2013) An intelligent model for visual scene analysis and compression, International Arab Journal of Information Technology, vol.10(13), pp. 126-136.
13. Lung, JWJ., Salam, MSH, Rehman, A., Rahim, MSM., Saba, T. (2014) Fuzzy phoneme classification using multi-speaker vocal tract length normalization, IETE Technical Review, vol. 31 (2), pp. 128-136, doi. 10.1080/02564602.2014.892669
14. Selamat, A. Phetchanchai, C. Saba, T. Rehman, A. (2010). Index financial time series based on zigzag-perceptually important points, Journal of Computer Science, vol. 6(12), pp. 1389-1395, doi. 10.3844/jcssp.2010.1389.1395.
15. Norouzi, A. Rahim, MSM, Altameem, A. Saba, T. Rada, A.E. Rehman, A. and Uddin, M. (2014) Medical image segmentation methods, algorithms, and applications IETE Technical Review, vol.31(3), pp. 199-213, doi. 10.1080/02564602.2014.906861.
16. Younus, Z.S. Mohamad, D. Saba, T. Alkawaz, M.H. Rehman, A. Al-Rodhaan, M. Al-Dhelaan, A. (2015) Content-based image retrieval using PSO and k-means clustering algorithm, Arabian Journal of Geosciences, vol. 8(8), pp. 6211-6224, doi. 10.1007/s12517-014-1584-7.
17. Rehman, A. Kurniawan, F. Saba, T. (2011) An automatic approach for line detection and removal without smash-up characters, The

- Imaging Science Journal, vol. 59(3), pp. 177-182, doi. 10.1179/136821910X12863758415649
18. Saba, T. Rehman, A. Sulong, G. (2010). Non-linear segmentation of touched roman characters based on genetic algorithm, International Journal of Computer Science and Engineering, vol 2(6),pp. 2167-2172.
 19. Al-Ameen, Z. Sulong, G. Rehman, A., Al-Dhelaan, A. Saba, T., Al-Rodhaan, M. (2015) An innovative technique for contrast enhancement of computed tomography images using normalized gamma-corrected contrast-limited adaptive histogram equalization, EURASIP Journal on Advances in Signal Processing:32. doi:10.1186/s13634-015-0214-1.
 20. Saba T, Al-Zahrani S, Rehman A. (2012) Expert system for offline clinical guidelines and treatment Life Sci Journal, vol.9(4), pp. 2639-2658.
 21. Muhsin; Z.F. Rehman, A.; Altameem, A.; Saba, A.; Uddin, M. (2014). Improved quadtree image segmentation approach to region information. the imaging science journal, vol. 62(1), pp. 56-62, doi. <http://dx.doi.org/10.1179/1743131X13Y.0000000063>.
 22. Haron, H. Rehman, A. Adi, DIS, Lim, S.P. and Saba, T.(2012). Parameterization method on B-Spline curve. mathematical problems in engineering, vol. 2012, doi:10.1155/2012/640472.
 23. Saba, T. Rehman, A. Elarbi-Boudihir, M. (2014). Methods and Strategies on Off-Line Cursive Touched Characters Segmentation: A Directional Review, Artificial Intelligence Review vol. 42 (4), pp. 1047-1066. doi 10.1007/s10462-011-9271-5
 24. Rad, A.E. Rahim,M.S.M, Rehman, A. Altameem, A. Saba, T. (2013) Evaluation of current dental radiographs segmentation approaches in computer-aided applications IETE Technical Review, vol. 30(3), pp. 210-222
 25. Joudaki, S. Mohamad, D. Saba, T. Rehman, A. Al-Rodhaan, M. Al-Dhelaan, A. (2014) Vision-based sign language classification: a directional Review, IETE Technical Review, vol.31(5), pp. 383-391, doi. 10.1080/02564602.2014.961576.
 26. M Elarbi-Boudihir, A Rehman, T Saba (2011) Video motion perception using optimized Gabor filter, International journal of physical sciences, vol.6(12),pp. 2799-2806.
 27. S Bekhti, A Rehman, M Al-Harbi, T Saba (2011) AQUASYS: An Arabic question-answering system based on extensive question analysis and answer relevance scoring, International Journal of Academic Research, vol.3(4), pp.45-51
 28. Saba, T. Rehman, A. Sulong, G. (2011) Cursive script segmentation with neural confidence, International Journal of Innovative Computing and Information Control (IJICIC), vol. 7(7), pp. 1-10.

4/7/2015